HHS Public Access

Author manuscript

Osteoporos Int. Author manuscript; available in PMC 2016 February 09.

Published in final edited form as:

Osteoporos Int. 2014 March ; 25(3): 973–982. doi:10.1007/s00198-013-2569-1.

Vertebral deformities and fractures are associated with MRI and pQCT measures obtained at the distal tibia and radius of postmenopausal women

C. S. Rajapakse, **E. A. Phillips**, **W. Sun**, **M. J. Wald**, **J. F. Magland**, **P. J. Snyder**, and **F. W. Wehrli**

University of Pennsylvania School of Medicine, Philadelphia, PA, USA

Abstract

Summary—We investigated the association of postmenopausal vertebral deformities and fractures with bone parameters derived from distal extremities using MRI and pQCT. Distal extremity measures showed variable degrees of association with vertebral deformities and fractures, highlighting the systemic nature of postmenopausal bone loss.

Introduction—Prevalent vertebral deformities and fractures are known to predict incident further fractures. However, the association of distal extremity measures and vertebral deformities in postmenopausal women has not been fully established.

Methods—This study involved 98 postmenopausal women (age range 60–88 years, mean 70 years) with DXA BMD T-scores at either the hip or spine in the range of −1.5 to −3.5. Wedge, biconcavity, and crush deformities were computed on the basis of spine MRI. Vertebral fractures were assessed using Eastell's criterion. Distal tibia and radius stiffness was computed using MRI-based finite element analysis. BMD at the distal extremities were obtained using pQCT.

Results—Several distal extremity MRI and pQCT measures showed negative association with vertebral deformity on the basis of single parameter correlation (r up to 0.67) and two-parameter regression (r up to 0.76) models involving MRI stiffness and pQCT BMD. Subjects who had at least one prevalent vertebral fracture showed decreased MRI stiffness (up to 17.9 %) and pQCT density (up to 34.2 %) at the distal extremities compared to the non-fracture group. DXA lumbar spine BMD T-score was not associated with vertebral deformities.

Conclusions—The association between vertebral deformities and distal extremity measures supports the notion of postmenopausal osteoporosis as a systemic phenomenon.

Keywords

Distal tibia and radius; Fracture; MRI; Osteoporosis; pQCT; Vertebral deformity

chamith@mail.med.upenn.edu.

Conflicts of interest None

Introduction

Vertebral fractures are among the most common outcomes of osteoporosis [1]. The prevalence of vertebral fractures is known to increase with age in both women and men (e.g., 50 % or more among women age 80 years or older) [2–4]. These fractures are associated with increased pain during day-to-day activities, reduced self-esteem, reduced mobility, and increased mortality [5, 6]. Prevalent vertebral fractures are known to predict incident vertebral [7–10] and non-spine fractures [11–14] independent of other fracture risk predictors such as BMD [15, 16]. The presence of both clinically overt (i.e., coming to clinical attention with the onset of pain) and clinically "silent" (i.e., asymptomatic) vertebral fractures (collectively termed morphometric fractures) can have substantial influence on the future fracture risk and associated morbidity [17–19].

Most vertebral fractures are asymptomatic [3, 20, 21], which are consequences of gradual changes in the vertebral shape. Vertebral deformities can be quantified by measuring the anterior, middle, and posterior heights of each vertebral body and classifying the type of deformity as wedge, biconcavity, or crush deformity [22, 23]. Quantitatively, a vertebral fracture can be defined by setting a threshold to the degree of vertebral deformity. Among older population, wedge, biconcavity, and crush deformity fractures account for about 50, 17, and 13 % of all prevalent factures, respectively, while about 20 % of fractures are of more complex nature [15].

In clinical practice, lateral radiographic projections of the spine are used as the standard for confirming the presence of osteoporotic vertebral fractures [24]. Vertebral fracture assessment, a tool based on lateral 2D dual-energy X-ray absorptiometry (DXA) scans, has also been shown to identify prevalent vertebral fractures [25]. Magnetic resonance imaging (MRI, a general purpose imaging modality of wide diffusion throughout the world) of the spine has also shown potential for quantifying vertebral deformities in the entire spine [22]. None of these techniques, however, provides information on cortical and trabecular bone microstructure, a key component of bone quality underlying vertebral fractures [26–31]. Mechanical assessment of the vertebral microstructure directly by imaging would therefore be highly desirable for noninvasive management of subjects with, or at risk for, vertebral fractures. This, unfortunately, is challenging in vivo due to signal-to-noise ratio limitations in MRI and radiation dose restrictions in X-ray-based techniques.

Distal extremities, on the other hand, do not have these imaging limitations. High-resolution MRI [32, 33] and high-resolution peripheral computed tomography (HR-pQCT) [34, 35] are two emerging technologies that permit noninvasive acquisition of distal skeletal images at resolutions adequate to resolve bone's three-dimensional microstructure. However, the usefulness of distal extremity measures in predicting vertebral fracture status has not been fully established. A number of studies have examined the role of cortical [36, 37] and trabecular [22, 23, 38–40] bone microstructure at extremities in association with vertebral fractures. In the absence of high-resolution imaging-based techniques to directly estimate the mechanical competence of the vertebrae in vivo, surrogate microstructural parameters obtained at distal sites using MRI [22, 23, 41] and HR-pQCT [34, 39, 42] have been shown to discriminate between fracture and non-fracture postmenopausal populations. Recently,

Liu et al. [40] reported that bone microstructure and stiffness measured by HR-pQCT of the distal radius and tibia parallel stiffness of the lumbar spine in premenopausal women. However, it is unclear how these distal extremity measures are associated with different types of vertebral deformities.

Since a vertebral fracture is inherently a manifestation of mechanical failure, the mechanical competence of the cortical and trabecular microstructure plays a major role in determining the fracture risk. It would therefore be useful to understand if there is an association between vertebral deformity and mechanical competence quantifiable at distal skeletal sites using noninvasive imaging techniques.

The goal of this study was to investigate if wedge, biconcavity, and crush deformities and fractures are associated with MRI-derived mechanical and pQCT-derived density measures obtained from distal tibia and radius on the basis of single parameter and combined regression models.

Methods

This is a retrospective biomechanical analysis of imaging data from a previously completed study involving bone's microstructural measures in postmenopausal women with wide range of vertebral deformity. Full details of the subject characteristics and image acquisition protocols are given in [22] and pertinent details are summarized here. The institutional review board approved the study protocol. Written informed consent was obtained from all subjects.

Subjects

This study involved 98 postmenopausal women (age range 60–88 years, mean and median 70 years) with DXA BMD T-scores at either the hip or spine in the range of −1.5 to −3.5. Subjects with the following characteristics were not included in the study: medications affecting mineral homeostasis (bisphosphonates within the previous 24 months, calcitonin within the previous 6 months, and use of ≥20 mg/day glucocorticoids for >2 weeks during the previous 6 months), hyperparathyroidism, gastrointestinal disease resulting in malabsorption, current alcohol use (>3 drinks/day), illicit drug use, gastric bypass, and Paget's disease.

Spine MRI acquisition

Vertebral deformity analysis was performed on the basis of the previously acquired sagittal MR images of the thoracolumbar spine by means of a fast spin-echo sequence (TR/TE of 4000/13.6 ms, echo train length 8, bandwidth 31.25 kHz, NEX 2, field of view 40×30 cm, longer side along the inferior–superior direction, 0.78 mm×0.78 mm pixel size, and variable number of slices of 5-mm thickness to correct for errors caused by scoliosis and sagittal obliquity).

Vertebral deformity quantification

Using custom-designed software written in IDL (Exelis, Inc., Boulder, CO), the stack of sagittal spine images were displayed, the image transecting each vertebra in the midline was located, and the four corners and midpoints of the inferior and superior edges of the vertebra were manually marked (Fig. 1a). Special precautions were taken in the measurement to avoid errors from osteophytes and depressions caused by endplate herniations (Schmorl's nodes). Anterior height (H_a), middle height (H_m), and posterior height (H_p) of each vertebra were computed by taking the Euclidian distance between landmark points. Three types of vertebral deformities were obtained by treating vertebral height ratios as continuous variables in the following manner:

1. Wedge deformity (anterior–posterior asymmetry)

$$W = (H_p/H_a - 1) \times 100\%$$

2. Biconcavity deformity (central depression)

$$B = (H_p/H_m - 1) \times 100\%$$

3. Crush deformity (compression relative to two neighboring vertebrae)

$$C = (<H>_{above} + <H>_{below})/2/<H> - 1) \times 100\%$$

where $<H> = (H_a + H_m + H_p)/3$

The total wedge, biconcavity, and crush deformities were computed as the mean deformity of vertebrae in the T4–L5 region. The number of analyzable vertebrae varied among subjects because for a fixed FOV the number of visible vertebrae is a function of subject's height.

Definition of vertebral fracture

Eastell's criterion [43] was used to identify vertebral fractures corresponding to each type of deformity for each vertebra by using a fracture threshold of three standard deviations below the arithmetic mean deformity of the reference population. This approach avoids classifying of non-fracture deformities (e.g., due to degenerative remodeling and Scheuermann's kyphosis, etc.) as fracture by considering the “normal” asymmetry in vertebral height ratios in healthy subjects [44, 45]. The normal reference deformity values for postmenopausal women were obtained from the spine images by computing the mean deformity values of the cohort by making sure that any outliers resulting from measurement error or image artifacts are not included, as suggested by Melton et al. and Black et al. [3, 46].

High-resolution MRI of distal radius and tibia

All high-resolution MRI scans had previously been obtained on a 1.5-T whole body clinical MRI scanner (Signa; General Electric, Milwaukee, WI, USA) using a 3D FLASE (fast large-angle spin-echo) pulse sequence with a flip angle of 140°, TR/TE 80/9.5 ms,

bandwidth 7.81 kHz, field of view 7 cm×4 cm×1.3 cm (radius) or 7 cm×5 cm×1.3 cm (tibia), and voxel size 137 μm×137 μm×410 μm (third dimension along the inferior–superior direction) from 60 subjects. The acquisition time was ~12 min for the radius and ~16 min for the tibia.

Image processing

Distal tibia and radius stiffness values were derived from MRI data using the following steps (Fig. 1b). The raw MRI data were corrected for translational shifts in the transverse plane resulting from involuntary subject motion during the scan using the navigator information collected during image acquisition [47]. Image intensity variations across the scan volume caused by spatially inhomogeneous sensitivity of the MR receive coil were corrected using a local thresholding algorithm [48]. Subsequently, an image volume corresponding to an 8-mm thick trans-axial slab was extracted from the 3D image dataset. The grayscale values of the images were linearly scaled to cover the range from 0 to 100 %, with pure marrow and pure bone having minimum and maximum values, respectively. We refer to the resulting 3D array as the bone–volume fraction map with individual voxel values representing the fraction of the voxel occupied by bone. Finally, three sets of 3D volumes, corresponding to cortical compartment, trabecular compartment, and total section were extracted by delineating the endosteal and periosteal boundaries on slice-by-slice basis and synchronizing across slices using a custom-designed operator-guided segmentation algorithm [49]. The coefficient of variation for the intra-operator reproducibility of mechanical parameters derived from segmented cortical and trabecular compartments was less than 3 %.

Finite-element model generation

Each voxel in the bone–volume fraction map was directly converted to a hexahedral finite element with dimensions equal to the voxel size [50]. Bone tissue was assumed to have an elastic modulus of 15 GPa and Poisson's ratio of 0.3 [51]. The elastic modulus assigned to each finite element was linearly scaled by the bone–volume fraction value of the corresponding voxel to account for partial volume effects in the limited spatial resolution regime of in vivo MRI. Three sets of finite element models corresponding to the cortical compartment, trabecular compartment, and total section were generated.

Bone stiffness computation

To estimate the axial stiffness of the cortical compartment, trabecular compartment, and total section encompassing the entire cross-section of the bone, compressive loading was simulated in the linear-elastic regime. A 1 % axial strain was applied to the proximal face of the finite element model while keeping the distal face constrained in the axial direction, assuming frictionless conditions along the transverse directions. The finite element nodes on lateral sides were not constrained, allowing 3 degrees of freedom. The finite element models were then solved by minimizing the total strain energy resulting in equilibrium displacements at each finite element node [52]. Axial stiffness was obtained as the ratio of the stress on the proximal face to the applied strain.

Bone densitometry

Peripheral quantitative computed tomography (pQCT, XCT 2000; Stratec, Pforzheim, Germany) had previously been performed in the metaphysis of the left tibia and radius proximal to the line of growth plate fusion by 17 and 11 mm, respectively, corresponding approximately to the sites of MRI. A single tomographic slice of 2.3-mm slice thickness was taken at a pixel size of 0.4×0.4 mm^2. Volumetric trabecular, cortical, and total bone mineral density (in grams per cubic centimeter) were computed with the manufacturer's software. Following the recommendations of the International Society for Clinical Densitometry, DXA was performed at the AP spine (L1–L4) and total hip to measure areal BMD (in grams per square centimeter) using a Hologic Discovery bone densitometer (version 12.3; Hologic, Bedford, MA, USA).

Statistical analysis

The normality of the distributions of the parameters was tested with the Shapiro–Wilk test. For correlation testing of normally distributed parameters, Pearson's correlation coefficient was used. Otherwise, Spearman's correlation coefficient was computed. Fisher r-to-z transformation was used to assess significant differences between correlation coefficients. MRI stiffness and pQCT density derived from the distal sites were used in a two-parameter linear regression model as separate predictor variables to investigate the predictability of vertebral deformities when combining mechanical information provided by MRI-based finite element analysis and bone mineral density measured using pQCT. Normality of error distributions was tested. More conservative, adjusted r values were reported. To test if parameters derived from the distal sites were significantly different between the vertebral fracture and non-fracture groups, t tests were used if the distributions were normal; otherwise, Wilcoxon tests were used. All t tests were two-sided and considered statistically significant if the p value was below 0.05. All analyses were conducted with the statistical package JMP 9.0.0 (SAS Institute, Cary, NC, USA).

Results

Associations between distal extremity bone measures and vertebral deformities

Several MRI and pQCT measures derived from the two distal sites were negatively correlated with vertebral deformities for all significant associations, indicating that decreased bone stiffness and density are reflective of increased vertebral deformity (Fig. 2). The strength of these associations varied across the types of measure, highlighting the complementary nature of information derived from MRI and pQCT. MRI-based distal tibia stiffness measures were associated with biconcavity and wedge vertebral deformities (r up to 0.67) but not with crush deformities. Distal radius stiffness, on the other hand, did not show significant associations with vertebral deformity measures, except for the moderate association between total radius stiffness and biconcavity deformity. All pQCT measures (except for tibia trabecular density) showed weak to moderate significant associations with at least one type of vertebral deformity.

Two-parameter regression model prediction of vertebral deformities

The combination of MRI stiffness with pQCT density obtained from the same distal skeletal region as independent variables in a two-parameter regression model showed significantly stronger association with vertebral deformity measures than did single parameter correlations, with adjusted r values up to 0.76 (Fig. 3).

Identification of vertebral fracture from distal extremity measurements

Subjects who had at least one prevalent vertebral fracture showed decreased MRI stiffness (up to 17.9 %, $p < 0.0005$) and pQCT density (up to 34.2 %, $p < 0.0005$) at the tibia and wrist compared to the non-fracture group (Fig. 4).

Spine BMD T-score classification of vertebral deformity

When subjects were classified into normal, osteopenic, and osteoporotic groups based on spine BMD T-scores using WHO criteria, none of the vertebral deformity measures showed significant differences between the three groups (Fig. 5), highlighting the limitations of spine BMD T-score in assessing vertebral deformities.

Discussion

This study made use of imaging data obtained previously by Ladinsky et al. [22] from a cohort of postmenopausal women. The prior study investigated the association between the total vertebral deformity and MRI-based trabecular bone structural measures of topology and scale at two distal sites—the distal radius and tibia. The focus of the present study was to extend that work by testing if wedge, biconcavity, and crush vertebral deformities and fractures separately are associated with mechanical and density parameters derived from the two distal sites.

The data showed that vertebral deformities and prevalent morphometric vertebral fractures are associated with several MRI and pQCT measures derived from distal extremities. This observation is in agreement with the notion that postmenopausal osteoporosis is a systemic disorder affecting the entire skeleton. Cortical as well as trabecular measures derived from the distal extremities showed associations with vertebral deformities and fracture. These associations are not surprising because vertebral deformities are manifestations of mechanical impairment of the cortical and trabecular network. A recent study by Liu et al. also reported that trabecular bone measures derived from distal extremities using HR-pQCT-based finite element analysis discriminate postmenopausal women with and without prevalent vertebral fractures [53].

Data further show that vertebral deformity was associated with MR-derived mechanical measures obtained from the distal tibia but not with the distal radius (except for the weak association between total stiffness and biconcavity deformity). This observation may be due to both vertebral column and tibia being load-bearing sites, thereby providing parallel mechanical stimulation [54] for maintaining bone strength. Furthermore, the distal tibia has a thinner cortex, thereby transmitting a greater fraction of load through the trabecular network (similar to vertebrae [55]) than does the axially loaded radius. The fact that vertebral deformities are associated with radial BMD but not with stiffness suggests that the

mechanical competence of non-load bearing sites (e.g., radius) does not necessarily reflect the mechanical consequences of load bearing sites (e.g., vertebral column).

Volumetric bone mineral densities derived from the same two distal sites also showed associations with vertebral deformities, further highlighting the systemic nature of postmenopausal bone loss. Interestingly, DXA spine BMD was not associated with any of the vertebral deformity measures, showing the inability of spine BMD to predict vertebral deformities. One possible explanation for the lack of association between vertebral deformity and BMD is that DXA BMD measurements are optimized and calibrated to work best for “normal” vertebrae. In the presence of vertebral deformity, the projected area of the vertebral bodies used to compute the areal BMD may not be measured accurately, thereby falsely elevating/lowering the measured BMD. Furthermore, DXA does not provide a complete picture of spinal deformity because it is typically performed only in the lumbar region thereby missing the deformities in the thoracic region. Analyzable vertebrae in DXA often get reduced even further due to artifacts caused by osteophytes and aortic calcifications.

This study highlights the synergistic effect of combining information from multiple modalities for vertebral deformity assessment. Combining MRI-derived mechanical measures with pQCT-derived density values (both obtained from matching distal skeletal regions) via a two-parameter regression model improved prediction of all three vertebral deformity types (adjusted r up to 0.76, $p < 0.0005$) significantly better than individual parameter estimates. This observation indicates that pQCT adds complementary volumetric density information to the regression model that cannot be obtained from conventional MRI involving structure imparted mechanical information provided by MRI-based finite element analysis. Currently, DXA BMD (in grams per square centimeter) is the only imaging-based parameter included in the WHO fracture assessment tool (FRAX). Future studies could investigate if inclusion of high-resolution MRI or HR-pQCT-derived parameters in FRAX could improve fracture predictions.

Several limitations should be considered alongside the study's findings. First, we defined vertebral fractures using a fracture threshold of three standard deviations below the arithmetic mean of the reference data. It should be noted that variability of vertebral height ratios in the reference cohort used and also measurement error influence the standard deviation and thereby determine the fracture threshold. However, it has been shown that these factors have limited impact on the diagnosis of vertebral fractures using the three standard deviations criterion [56]. Second, although the data suggest that parameters obtained from the distal sites are associated with the vertebral deformities and fractures, the results cannot be extrapolated to predict future vertebral fractures because the study design was cross-sectional. Furthermore, since prevalent vertebral fracture is a risk factor for future vertebral fractures through mechanical coupling of each vertebra, the severity of deformity and number of fractures could have a nonlinear relationship with time.

Although bone's microstructural properties vary throughout the skeleton [57], measures of bone quality representative of density and strength, quantified at the two distal extremities, were associated with vertebral deformities and fractures to a variable degree in

postmenopausal women. Furthermore, the fact that these associations were different for the three deformity types suggest that vertebral fracture patterns have to be considered when assessing vertebral deformities using surrogate measures obtained from other skeletal locations. The association between vertebral deformities and volumetric measures of cortical and trabecular bone derived from distal skeletal imaging (in addition to the bone-quality measures derived from the same distal sites) could potentially provide insight on how aggressively to pursue treatment to reduce future fractures by redefining the intervention thresholds currently based only on BMD and clinical risk factors. Such an approach could be particularly appealing for individuals with osteopenia (more than those with a history of fracture or osteoporosis) because of the current lack of effective criteria for identifying fracture risk [58] while limiting the risks associated with antiresorptive drug therapy. However, this hypothesis requires verification by a large prospective study.

Acknowledgments

Research reported in this publication was supported by the National Institute of Arthritis and Musculoskeletal and Skin Diseases of the National Institutes of Health under award numbers RO1 AR49553 and K25 AR 060283 and the content is solely the responsibility of the authors and does not necessarily represent the official views of the National Institutes of Health.

References

1. Cummings SR, Black DM, Rubin SM. Lifetime risks of hip, Colles', or vertebral fracture and coronary heart disease among white postmenopausal women. Arch Intern Med. 1989; 149:2445–2448. [PubMed: 2818106]
2. Melton LJ 3rd, Kan SH, Frye MA, Wahner HW, O'Fallon WM, Riggs BL. Epidemiology of vertebral fractures in women. Am J Epidemiol. 1989; 129:1000–1011. [PubMed: 2784934]
3. Melton LJ 3rd, Lane AW, Cooper C, Eastell R, O'Fallon WM, Riggs BL. Prevalence and incidence of vertebral deformities. Osteoporos Int. 1993; 3:113–119. [PubMed: 8481586]
4. O'Neill TW, Felsenberg D, Varlow J, Cooper C, Kanis JA, Silman AJ. The prevalence of vertebral deformity in European men and women: the European Vertebral Osteoporosis Study. J Bone Miner Res. 1996; 11:1010–1018. [PubMed: 8797123]
5. Goh S, Tan C, Price RI, Edmondston SJ, Song S, Davis S, Singer KP. Influence of age and gender on thoracic vertebral body shape and disc degeneration: an MR investigation of 169 cases. J Anat. 2000; 197(Pt 4):647–657. [PubMed: 11197538]
6. Kado DM, Duong T, Stone KL, Ensrud KE, Nevitt MC, Greendale GA, Cummings SR. Incident vertebral fractures and mortality in older women: a prospective study. Osteoporos Int. 2003; 14:589–594. [PubMed: 12827222]
7. Klotzbuecher CM, Ross PD, Landsman PB, Abbott TA 3rd, Berger M. Patients with prior fractures have an increased risk of future fractures: a summary of the literature and statistical synthesis. J Bone Miner Res. 2000; 15:721–739. [PubMed: 10780864]
8. Melton LJ 3rd, Atkinson EJ, Cooper C, O'Fallon WM, Riggs BL. Vertebral fractures predict subsequent fractures. Osteoporos Int. 1999; 10:214–221. [PubMed: 10525713]
9. Ross PD, Genant HK, Davis JW, Miller PD, Wasnich RD. Predicting vertebral fracture incidence from prevalent fractures and bone density among non-black, osteoporotic women. Osteoporos Int. 1993; 3:120–126. [PubMed: 8481587]
10. Schousboe JT, Fink HA, Lui LY, Taylor BC, Ensrud KE. Association between prior non-spine non-hip fractures or prevalent radiographic vertebral deformities known to be at least 10 years old and incident hip fracture. J Bone Miner Res. 2006; 21:1557–1564. [PubMed: 16995810]
11. Burger H, Vandaele PLA, Algra D, Hofman A, Grobbee DE, Schutte HE, Birkenhager JC, Pols HAP. Vertebral deformities as predictors of non-vertebral fractures. Br Med J. 1994; 309:991–992. [PubMed: 7950721]

12. Haentjens P, Autier P, Collins J, Velkeniers B, Vanderschueren D, Boonen S. Colles fracture, spine fracture, and subsequent risk of hip fracture in men and women. A meta-analysis. J Bone Joint Surg. 2003; 85-A:1936–1943. [PubMed: 14563801]

13. Ismail AA, Cockerill W, Cooper C, Finn JD, Abendroth K, Parisi G, Banzer D, Benevolenskaya LI, Bhalla AK, Armas JB, Cannata JB, Delmas PD, Dequeker J, Dilsen G, Eastell R, Ershova O, Falch JA, Felsch B, Havelka S, Hoszowski K, Jajic I, Kragl U, Johnell O, Vaz AL, Lorenc R, Lyritis G, Marchand F, Masaryk P, Matthis C, Miazgowski T, Pols HAP, Poor G, Rapado A, Raspe HH, Reid DM, Reisinger W, Janott J, Scheidt-Nave C, Stepan J, Todd C, Weber K, Woolf AD, Ambrecht G, Gowin W, Felsenberg D, Lunt M, Kanis JA, Reeve J, Silman AJ, O'Neill TW. Prevalent vertebral deformity predicts incident hip though not distal forearm fracture: Results from the European Prospective Osteoporosis Study. Osteoporos Int. 2001; 12:85–90. [PubMed: 11303719]

14. Johnell O, Oden A, Caulin F, Kanis JA. Acute and long-term increase in fracture risk after hospitalization for vertebral fracture. Osteoporos Int. 2001; 12:207–214. [PubMed: 11315239]

15. Black DM, Arden NK, Palermo L, Pearson J, Cummings SR. Prevalent vertebral deformities predict hip fractures and new vertebral deformities but not wrist fractures. Study of Osteoporotic Fractures Research Group. J Bone Miner Res. 1999; 14:821–828. [PubMed: 10320531]

16. Ross PD, Davis JW, Epstein RS, Wasnich RD. Preexisting fractures and bone mass predict vertebral fracture incidence in women. Ann Intern Med. 1991; 114:919–923. [PubMed: 2024857]

17. Fink HA, Ensrud KE, Nelson DB, Kerani RP, Schreiner PJ, Zhao Y, Cummings SR, Nevitt MC. Disability after clinical fracture in postmenopausal women with low bone density: the fracture intervention trial (FIT). Osteoporos Int. 2003; 14:69–76. [PubMed: 12577187]

18. Nevitt MC, Ettinger B, Black DM, Stone K, Jamal SA, Ensrud K, Segal M, Genant HK, Cummings SR. The association of radiographically detected vertebral fractures with back pain and function: a prospective study. Ann Intern Med. 1998; 128:793–800. [PubMed: 9599190]

19. O'Neill TW, Cockerill W, Matthis C, Raspe HH, Lunt M, Cooper C, Banzer D, Cannata JB, Naves M, Felsch B, Felsenberg D, Janott J, Johnell O, Kanis JA, Kragl G, Vaz AL, Lyritis G, Masaryk P, Poor G, Reid DM, Reisinger W, Scheidt-Nave C, Stepan JJ, Todd CJ, Woolf AD, Reeve J, Silman AJ. Back pain, disability, and radiographic vertebral fracture in European women: a prospective study. Osteoporos Int. 2004; 15:760–765. [PubMed: 15138664]

20. Cooper C, O'Neill T, Silman A. The epidemiology of vertebral fractures. European Vertebral Osteoporosis Study Group. Bone. 1993; 14(Suppl 1):S89–S97. [PubMed: 8110529]

21. Fink HA, Milavetz DL, Palermo L, Nevitt MC, Cauley JA, Genant HK, Black DM, Ensrud KE. What proportion of incident radiographic vertebral deformities is clinically diagnosed and vice versa? J Bone Miner Res. 2005; 20:1216–1222. [PubMed: 15940375]

22. Ladinsky GA, Vasilic B, Popescu AM, Wald M, Zemel BS, Snyder PJ, Loh L, Song HK, Saha PK, Wright AC, Wehrli FW. Trabecular structure quantified with the MRI-based virtual bone biopsy in postmenopausal women contributes to vertebral deformity burden independent of areal vertebral BMD. J Bone Miner Res. 2008; 23:64–74. [PubMed: 17784842]

23. Wehrli FW, Gomberg BR, Saha PK, Song HK, Hwang SN, Snyder PJ. Digital topological analysis of in vivo magnetic resonance microimages of trabecular bone reveals structural implications of osteoporosis. J Bone Miner Res. 2001; 16:1520–1531. [PubMed: 11499875]

24. Grigoryan M, Guermazi A, Roemer FW, Delmas PD, Genant HK. Recognizing and reporting osteoporotic vertebral fractures. Eur Spine J. 2003; 12(Suppl 2):S104–S112. [PubMed: 13680316]

25. Rosen HN, Vokes TJ, Malabanan AO, Deal CL, Alele JD, Olenginski TP, Schousboe JT. Vertebral Fracture Assessment: The 2013 Official Positions. J Clin Densitom. 2013

26. Fields AJ, Eswaran SK, Jekir MG, Keaveny TM. Role of trabecular microarchitecture in whole-vertebral body biomechanical behavior. J Bone Miner Res. 2009; 24:1523–1530. [PubMed: 19338454]

27. Genant HK, Delmas PD, Chen P, Jiang Y, Eriksen EF, Dalsky GP, Marcus R, San Martin J. Severity of vertebral fracture reflects deterioration of bone microarchitecture. Osteoporos Int. 2007; 18:69–76. [PubMed: 17028792]

28. Kleerekoper M, Villanueva AR, Stanciu J, Rao DS, Parfitt AM. The role of three-dimensional trabecular microstructure in the pathogenesis of vertebral compression fractures. Calcif Tissue Int. 1985; 37:594–597. [PubMed: 3937580]
29. Legrand E, Chappard D, Pascaretti C, Duquenne M, Krebs S, Rohmer V, Basle MF, Audran M. Trabecular bone microarchitecture, bone mineral density, and vertebral fractures in male osteoporosis. J Bone Miner Res. 2000; 15:13–19. [PubMed: 10646109]
30. Parfitt AM. Implications of architecture for the pathogenesis and prevention of vertebral fracture. Bone. 1992; 13(Suppl 2):S41–S47. [PubMed: 1627414]
31. Recker RR. Architecture and vertebral fracture. Calcif Tissue Int. 1993; 53(Suppl 1):S139–S142. [PubMed: 8275368]
32. Majumdar S. Magnetic resonance imaging for osteoporosis. Skelet Radiol. 2008; 37:95–97.
33. Wehrli FW. Structural and functional assessment of trabecular and cortical bone by micromagnetic resonance imaging. J Magn Reson Imaging. 2007; 25:390–409. [PubMed: 17260403]
34. Boutroy S, Bouxsein ML, Munoz F, Delmas PD. In vivo assessment of trabecular bone microarchitecture by high-resolution peripheral quantitative computed tomography. J Clin Endocrinol Metab. 2005; 90:6508–6515. [PubMed: 16189253]
35. Laib, A.; Hammerle, S.; Koller, B. A new 100-μm resolution scanner for in vivo 3D-CT of the human forearm and lower leg. 16th International Bone Densitometry workshop; 2004.
36. Sornay-Rendu E, Boutroy S, Munoz F, Bouxsein ML. Cortical and trabecular architecture are altered in postmenopausal women with fractures. Osteoporos Int. 2009; 20:1291–1297. [PubMed: 19590838]
37. Sornay-Rendu E, Cabrera-Bravo JL, Boutroy S, Munoz F, Delmas PD. Severity of vertebral fractures is associated with alterations of cortical architecture in postmenopausal women. J Bone Miner Res. 2009; 24:737–743. [PubMed: 19113929]
38. Link TM, Vieth V, Matheis J, Newitt D, Lu Y, Rummeny EJ, Majumdar S. Bone structure of the distal radius and the calcaneus versus BMD of the spine and proximal femur in the prediction of osteoporotic spine fractures. Eur Radiol. 2002; 12:401–408. [PubMed: 11870442]
39. Melton LJ 3rd, Riggs BL, Keaveny TM, Achenbach SJ, Hoffmann PF, Camp JJ, Rouleau PA, Bouxsein ML, Amin S, Atkinson EJ, Robb RA, Khosla S. Structural determinants of vertebral fracture risk. J Bone Miner Res. 2007; 22:1885–1892. [PubMed: 17680721]
40. Liu XS, Cohen A, Shane E, Yin PT, Stein EM, Rogers H, Kokolus SL, McMahon DJ, Lappe JM, Recker RR, Lang T, Guo XE. Bone density, geometry, microstructure, and stiffness: relationships between peripheral and central skeletal sites assessed by DXA, HR-pQCT, and cQCT in premenopausal women. J Bone Miner Res. 2010; 25:2229–2238. [PubMed: 20499344]
41. Wehrli FW, Hwang SN, Ma J, Song HK, Ford JC, Haddad JG. Cancellous bone volume and structure in the forearm: noninvasive assessment with MR microimaging and image processing. Radiology. 1998; 206:347–357. [PubMed: 9457185]
42. Sornay-Rendu E, Boutroy S, Munoz F, Delmas PD. Alterations of cortical and trabecular architecture are associated with fractures in postmenopausal women, partially independent of decreased BMD measured by DXA: the OFELY study. J Bone Miner Res. 2007; 22:425–433. [PubMed: 17181395]
43. Eastell R, Cedel SL, Wahner HW, Riggs BL, Melton LJ 3rd. Classification of vertebral fractures. J Bone Miner Res. 1991; 6:207–215. [PubMed: 2035348]
44. Davies KM, Recker RR, Heaney RP. Normal vertebral dimensions and normal variation in serial measurements of vertebrae. J Bone Miner Res. 1989; 4:341–349. [PubMed: 2763872]
45. Jackson SA, Tenenhouse A, Robertson L. Vertebral fracture definition from population-based data: preliminary results from the Canadian Multicenter Osteoporosis Study (CaMos). Osteoporos Int. 2000; 11:680–687. [PubMed: 11095171]
46. Black DM, Cummings SR, Stone K, Hudes E, Palermo L, Steiger P. A new approach to defining normal vertebral dimensions. J Bone Miner Res. 1991; 6:883–892. [PubMed: 1785377]
47. Song HK, Wehrli FW. In vivo micro-imaging using alternating navigator echoes with applications to cancellous bone structural analysis. Magn Reson Med. 1999; 41(5):947–53. PubMed PMID: 10332878. [PubMed: 10332878]

48. Vasilic B, Wehrli FW. A novel local thresholding algorithm for trabecular bone volume fraction mapping in the limited spatial resolution regime of in vivo MRI. IEEE Trans Med Imaging. 2005; 24(12):1574–85. PubMed PMID:16353372. [PubMed: 16353372]

49. Rajapakse CS, Leonard MB, Bhagat YA, Sun W, Magland JF, Wehrli FW. Micro-MR imaging-based computational biomechanics demonstrates reduction in cortical and trabecular bone strength after renal transplantation. Radiology. 2012; 262:912–920. [PubMed: 22357891]

50. Rajapakse CS, Magland JF, Wald MJ, Liu XS, Zhang XH, Guo XE, Wehrli FW. Computational biomechanics of the distal tibia from high-resolution MR and micro-CT images. Bone. 2010; 47:556–563. [PubMed: 20685323]

51. Guo XE, Goldstein SA. Is trabecular bone tissue different from cortical bone tissue? Forma. 1997; 12:185–196.

52. Magland JF, Zhang N, Rajapakse CS, Wehrli FW. Computationally-optimized bone mechanical modeling from high-resolution structural images. PloS one. 2012; 7:e35525. [PubMed: 22558164]

53. Liu XS, Wang J, Zhou B, Stein E, Shi X, Adams M, Shane E, Guo XE. Fast trabecular bone strength predictions of HR-pQCT and individual trabeculae segmentation (ITS)-based plate and rod finite element model discriminate postmenopausal vertebral fractures. J Bone Miner Res. 2013

54. Ozcivici E, Luu YK, Adler B, Qin YX, Rubin J, Judex S, Rubin CT. Mechanical signals as anabolic agents in bone. Nat Rev. 2009; 6:50–59.

55. Eswaran SK, Gupta A, Adams MF, Keaveny TM. Cortical and trabecular load sharing in the human vertebral body. J Bone Miner Res. 2006; 21:307–314. [PubMed: 16418787]

56. Szulc P, Munoz F, Sornay-Rendu E, Paris E, Souhami E, Zanchetta J, Bagur A, van der Mooren MJ, Young S, Delmas PD. Comparison of morphometric assessment of prevalent vertebral deformities in women using different reference data. Bone. 2000; 27:841–846. [PubMed: 11113396]

57. Eckstein F, Matsuura M, Kuhn V, Priemel M, Muller R, Link TM, Lochmuller EM. Sex differences of human trabecular bone microstructure in aging are site-dependent. J Bone Miner Res. 2007; 22:817–824. [PubMed: 17352643]

58. Schousboe JT, DeBold CR, Bowles C, Glickstein S, Rubino RK. Prevalence of vertebral compression fracture deformity by X-ray absorptiometry of lateral thoracic and lumbar spines in a population referred for bone densitometry. J Clin Densitom. 2002; 5:239–246. [PubMed: 12357061]

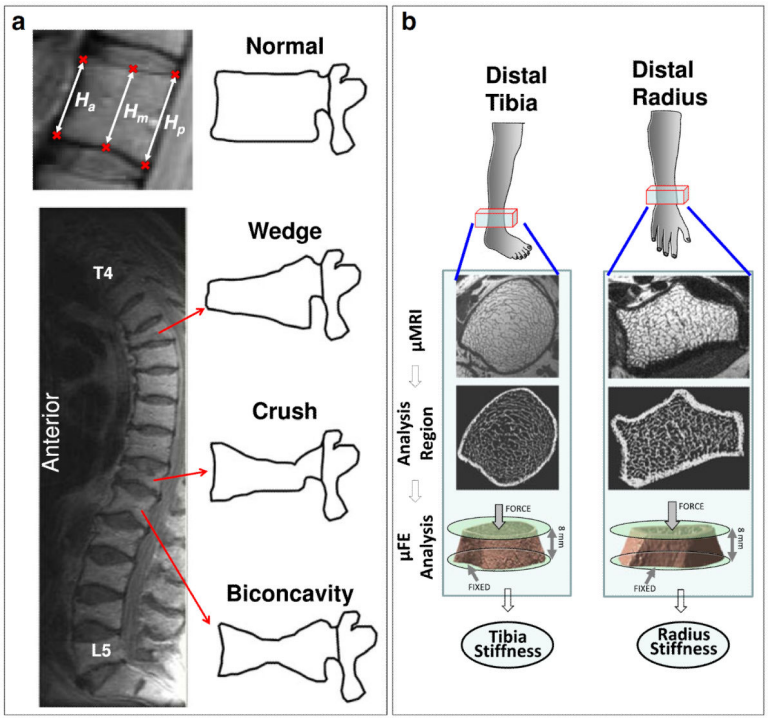

Fig. 1.

Illustration of **a** vertebral morphometric measurements showing the definitions of wedge, biconcavity, and crush deformity types derived from anterior (H_a), middle (H_m), and posterior (H_p) vertebral heights; and **b** acquisition of tibial and radial MR images, analysis region showing the bone–volume fraction maps, and computation of stiffness using finite element analysis

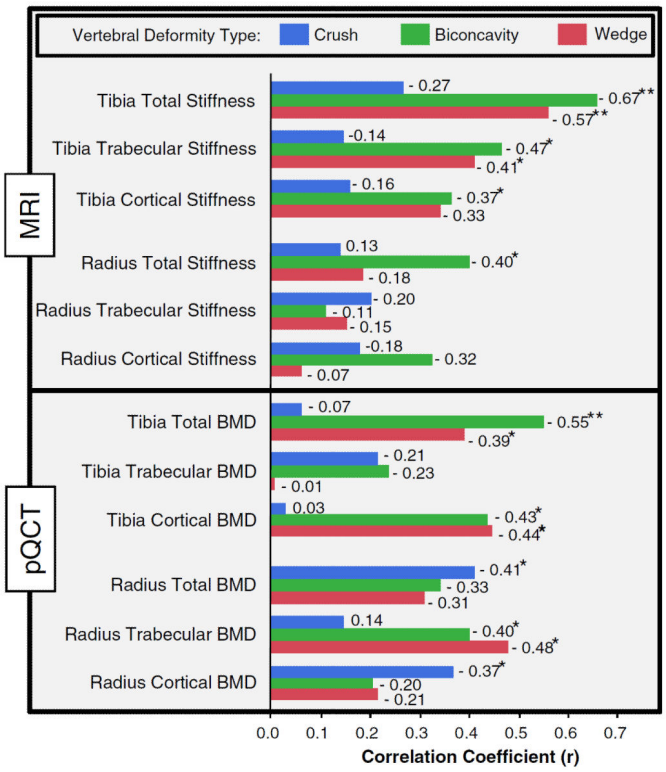

Fig. 2.

Correlation coefficients for the association between vertebral deformities and parameters derived from the two distal sites using MRI and pQCT. *Blue*, *green*, and *red* represent the association for the crush, biconcavity, and wedge vertebral deformities, respectively. Significance of the associations is indicated by *single* (p <0.05) and *double* (p <0.005) *asterisks*

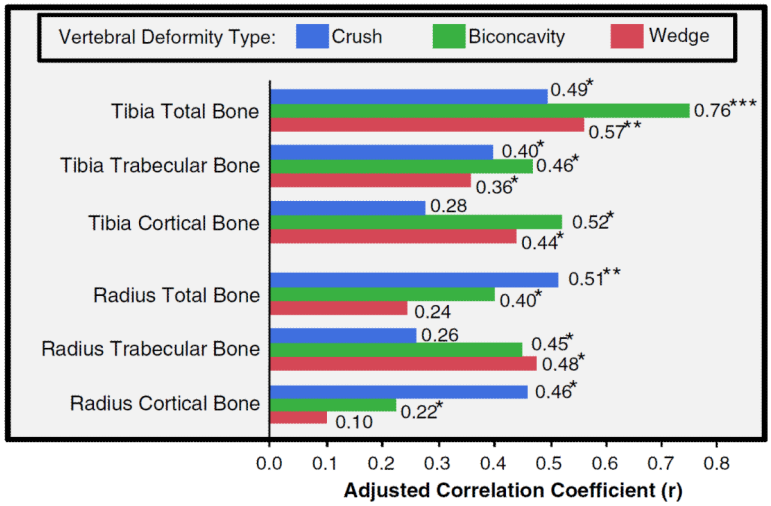

Fig. 3.

Correlation coefficient for the two-parameter regression model involving MRI stiffness and pQCT density as predictors of crush, biconcavity, and wedge deformities. Significance of the associations is indicated by *single* (p <0.05), *double* (p <0.005), and *triple* (p <0.0005) *asterisks*

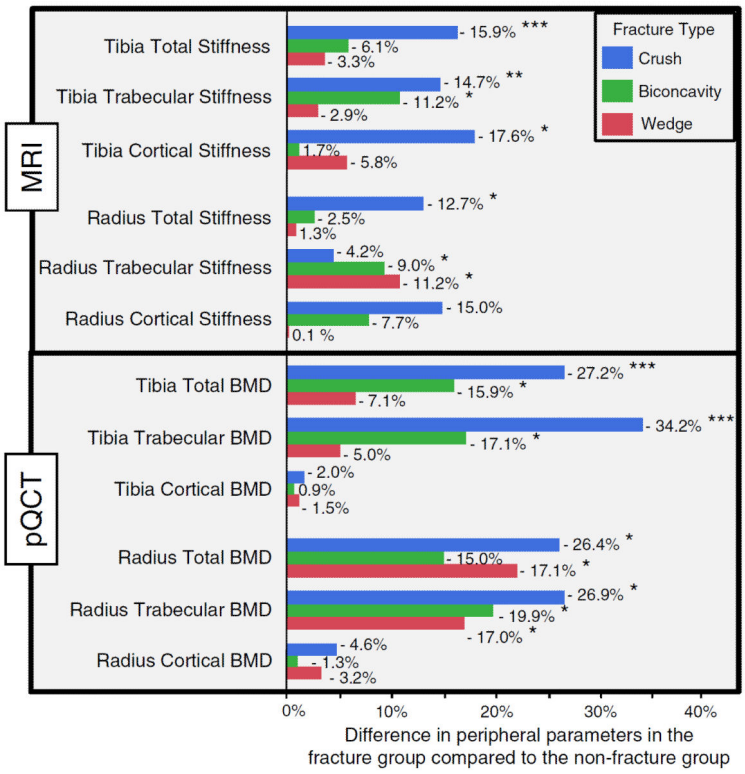

Fig. 4.

Mean percentage difference in distal-extremity measures between subjects having at least one vertebral fracture and non-fracture group, stratified according to the type of fracture. Negative values indicate decreased MRI stiffness and pQCT densities in the fracture group compared to the non-fracture group for the three types of fracture. Significance differences are indicated by *single* (p <0.05), *double* (p <0.005), and *triple* (p <0.0005) *asterisks*

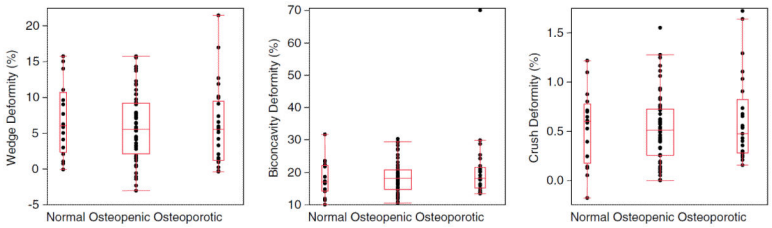

Fig. 5.

Comparison of wedge, biconcavity, and crush deformities among normal, osteopenic, and osteoporotic groups defined by the WHO spine BMD criterion showing no significant differences among the three groups